SEBHA UNIVERSITY CONFERENCE PROCEEDINGS, VOL.5 NO. 1 2026
DOI: 10.51984/9H1TF941

وقائع مؤتمرات جامعة سبها
Sebha University Conference Proceedings

Confrence Proceeeding homepage: http://www.sebhau.edu.ly/journal/CAS

Design and Analysis of a High-Isolation Dual-Element MIMO Microstrip Antenna with DGS for 5G and Futuristic Trends of 6G

Alaa Mustafa Dirbal[1], Marai Mohammed Abousetta[2]

[1] The Libyan Academy for Graduate Studies, Tripoli, Libya
[2] The Libyan Academy for Graduate Studies, Tripoli, Libya

Keywords:
5G/6G
MIMO antenna
Microstrip
mmWave
DGS
Slot-loading

ABSTRACT

In this work, we present the design evolution and performance evaluation of a compact dual-element MIMO microstrip antenna for mmWave 5G/6G applications. Starting from a basic patch geometry on Rogers RT5880 substrate, the design employs a dual-modification strategy: slot-loading the radiating patches to precisely tune the resonance and enhance gain, combined with multiple defected ground structures (DGS) to suppress mutual coupling and broaden the bandwidth. The antenna exhibits excellent reflection coefficients (S11, S22) below –25 dB at 27 GHz. Its -10 dB impedance bandwidth (VSWR < 2) is 1.312 GHz centered at 27 GHz. At 27 GHz, it achieves a VSWR of ~1.116, realized gain of 10.45 dBi, total efficiency of 78.5%, and directional radiation with half-power beamwidths of 50.0° (H-plane) and 34.1° (E-plane). These results demonstrate that the proposed antenna offers compact size, high isolation, excellent MIMO performance, and enhanced bandwidth, making it a strong candidate for next-generation mmWave wireless systems.

تصميم وتحليل هوائي MIMO ثنائي العنصر ذو عزل عالٍ مع هيكل أرضي معيب (DGS) لتطبيقات الجيل الخامس والاتجاهات المستقبلية للجيل السادس

الاء مصطفى دربال[1]، مرعي محمد أبوستة[2]

[1] الأكاديمية الليبية للدراسات العليا، طرابلس ، ليبيا
[2] الأكاديمية الليبية للدراسات العليا، طرابلس، ليبيا

الكلمات المفتاحية:
الجيل الخامس/السادس
الموجات المليمترية
الهيكل الأرضي المعيب
تحميل الفتحات
شريطي دقيق
هوائي

الملخص

في هذا العمل، نعرض تطور تصميم وتقييم أداء هوائي ميكروستريب ثنائي العناصر بتقنية MIMO، صغير الحجم، لتطبيقات الجيل الخامس والسادس بتقنية الموجات المليمترية. انطلاقًا من هندسة رقعة أساسية على ركيزة Rogers RT5880، يعتمد التصميم على استراتيجية تعديل مزدوجة: تحميل الرقع المشعة بفتحات لضبط الرنين بدقة وتعزيز الكسب، بالإضافة إلى استخدام هياكل أرضية معيبة متعددة (DGS) لتخميد الاقتران المتبادل وزيادة عرض النطاق الترددي. يُظهر الهوائي معاملات انعكاس ممتازة (S11، S22) أقل من -25 ديسيبل عند 27 جيجاهرتز. يبلغ عرض نطاق المعاوقة -10 ديسيبل (1.312 (VSWR < 2 جيجاهرتز، متمركزًا عند 27 جيجاهرتز. يحقق الهوائي نسبة موجة واقفة (VSWR) تبلغ حوالي 1.116، وكسب قدره 10.45 ديسيبل، وكفاءة إجمالية تبلغ 78.5%، وإشعاعًا اتجاهيًا بعرض حزمة نصف القدرة 50.0° (في المستوى H) و34.1° (في المستوى E). تُظهر هذه النتائج أن الهوائي المقترح يتميز بحجمه الصغير، وعزله العالي، وأدائه الممتاز في تقنية MIMO، ، مما يجعله خيارًا مناسباً لأنظمة الموجات المليمترية اللاسلكية من الجيل التالي.

Introduction

The relentless advancement of wireless communication technologies has ushered in the era of fifth-generation (5G) networks and is actively paving the way for the visionary sixth-generation (6G) paradigm [1]. These next-generation systems are engineered to deliver transformative capabilities, including multi-gigabit-per-second data rates, sub-millisecond ultra-low latency, massive machine-type connectivity, and near-perfect reliability [2]. To materialize these ambitious benchmarks, the synergistic convergence of two pivotal technological pillars is essential: Multiple-Input Multiple-Output (MIMO) architectures and the exploitation of the millimeter-wave

*Corresponding author:
E-mail addresses: alamustafa436@gmail.com , (M. M. Abousetta) m.abousetta@academy.ly
Article History : Received 10 March 2026 - Received in revised form 15 April 2026 - Accepted 16 May 2026

(mmWave) frequency spectrum [3].

MIMO technology capitalizes on spatial multiplexing and diversity gains by deploying multiple antenna elements at both link ends, thereby dramatically enhancing spectral efficiency and link robustness without demanding additional bandwidth or increased transmit power [4]. Concurrently, the strategic migration to mmWave bands (typically spanning 24 GHz to 100 GHz) alleviates the acute spectral congestion plaguing conventional sub-6 GHz bands, unlocking vast swathes of contiguous bandwidth indispensable for supporting terabits-per-second-level aggregate throughput [5]. Within this mmWave landscape, the 28 GHz frequency has been globally identified by major regulatory bodies (e.g., the FCC in the USA) and standardization consortia (e.g., 3GPP) as a prime candidate for initial 5G New Radio (NR) deployments and a foundational band for 6G evolution, owing to its favorable compromise between atmospheric attenuation and available channel bandwidth [6].

However, the practical realization of high-performance MIMO systems within the mmWave regime, especially when constrained by the stringent form factors of contemporary user equipment (UEs), base stations, and access points, introduces profound design challenges [7]. The principal impediment originates from undesired mutual electromagnetic coupling between densely spaced radiating elements. This parasitic interaction precipitates a cascade of performance-degrading phenomena: it diminishes overall radiation efficiency by recirculating energy between ports instead of radiating it into free space; induces port impedance mismatch, leading to reflected power and reduced power transfer; distorts far-field radiation patterns, which undermines beamforming fidelity and spatial diversity gains; and elevates the envelope correlation coefficient (ECC), effectively eroding the theoretical channel capacity improvements promised by MIMO theory [8]. Consequently, the quest to achieve high inter-element isolation while preserving minimal antenna footprint and design simplicity has emerged as a critical and vibrant research domain in modern antenna engineering.

Sustained research endeavors have yielded a rich taxonomy of techniques aimed at mitigating mutual coupling in MIMO arrays, which can be systematically classified into three overarching methodologies. The first category emphasizes wave suppression via strategic structural modifications to the antenna environment. This encompasses the integration of Electromagnetic Band-Gap (EBG) structures periodic lattices that inhibit surface-wave propagation within specific frequency stopbands [9]; the deployment of metamaterial-inspired superstrates or metasurfaces that engineer the near-field distribution to reduce coupling [10]; and the implementation of Defected Ground Structures (DGS). DGS techniques involve etching specific patterns (slots, dumbbells, spirals) into the common ground plane to perturb and lengthen the path of shared surface currents, thereby weakening the coupling mechanism [11]–[13]. While frequently effective, these approaches often introduce additional design complexity, elevate fabrication costs, and may necessitate extra lateral or vertical space, counteracting miniaturization goals.

The second methodological school focuses on establishing a controlled compensatory coupling path engineered to destructively interfere with the innate mutual coupling. Techniques under this umbrella include neutralization lines direct conductive links between antenna feeds that carry a cancellation signal 180° out-of-phase [14]; strategically placed parasitic scatterers or resonators that reconfigure the local near-field environment [15]; and more elaborate decoupling networks employing transmission line sections or lumped-element circuits to achieve port matching and isolation simultaneously [16]. Although capable of delivering substantial isolation enhancement, these methods frequently demand meticulous tuning, increase overall circuit complexity, and may inadvertently compromise impedance bandwidth or radiation efficiency.

Driven by the limitations of additive structures, a third and increasingly prominent paradigm of self-decoupling or self-isolation techniques has crystallized. These elegant methods ingeniously exploit the innate electromagnetic properties of the antenna elements themselves leveraging modal orthogonality, strategic current distribution, or structural asymmetry to achieve high isolation intrinsically, without appending external decoupling components. Exemplary strategies in this vein include mode cancellation via judicious feed positioning to excite decoupled characteristic modes [17], the deliberate excitation of orthogonal mode pairs (e.g., TM_{10} and TM_{01}) in adjacent patches [18], and the creation of electric-field nulls at the coupling region through characteristic mode analysis (CMA) of the ground plane or radiator [19]. Recent avant-garde approaches have also explored sophisticated mode conversion mechanisms using embedded vias or etched slots to transform the operational mode of the patch, thereby inducing orthogonality with modes excited in neighboring elements [20]. Additionally, slot-loading techniques applied directly to the patch conductor have been used to tailor individual element performance, such as resonance frequency and bandwidth [21].

While these self-decoupling techniques are promising, a critical survey of the literature reveals two salient gaps this work aims to address. First, many state-of-the-art designs demonstrating exceptional isolation are validated primarily at lower microwave frequencies (e.g., sub-6 GHz, 5.8 GHz) [17]–[20], and their performance scalability to the mmWave regime often remains unverified or presents challenges related to fabrication tolerance and conductor/surface-wave losses. Second, several high-performance techniques, including the sophisticated annular via-based mode conversion method detailed in [20], achieve remarkable isolation but inherently demand complex, multi-layer geometries or precise vertical interconnects (vias), which increase manufacturing complexity, cost, and potential yield issues factors particularly sensitive for high-volume, cost-conscious consumer mmWave devices.

This paper directly confronts these identified challenges by introducing a compact, two-element MIMO microstrip patch antenna engineered for high-isolation and enhanced-bandwidth operation specifically within the 27 GHz mmWave band. Our central contribution is the demonstration that exceptional isolation (>38 dB) coupled with superior MIMO diversity performance (ECC $< 4\times10^{-7}$) and significantly improved impedance bandwidth (1.3124 GHz) can be attained using an elegantly simple, fully planar, and single-layer design philosophy. The proposed antenna achieves this through an enhanced dual-feature approach: the strategic incorporation of slots within each patch to optimize element performance, combined with multiple Defected Ground Structures (DGS) comprising one longitudinal slit and four additional rectangular slots etched into the shared ground plane. The proposed antenna, therefore, embodies a balanced and pragmatic synthesis of high electrical performance, enhanced bandwidth, and manufacturing simplicity, presenting itself as a viable and attractive candidate for integration into the next generation of compact wireless terminals operating in the 27 GHz 5G/6G landscape.

Antenna Design and Configuration

1 Substrate and Material Properties

The proposed dual-element MIMO antenna is fabricated on a Rogers RT5880 substrate, selected for its superior high-frequency characteristics and low-loss properties essential for millimeter-wave applications. The substrate exhibits a low relative permittivity (ε_r) of 2.2, an extremely low loss tangent (tan δ) of 0.0009, and a thickness (h) of 0.762 mm. The increased substrate thickness compared to conventional designs was deliberately chosen to enhance the impedance bandwidth while maintaining mechanical stability. These parameters ensure minimal dielectric losses and reduced surface wave propagation, which is critical at 27 GHz. The overall substrate dimensions are $40\times16.5\times0.832$ mm^3 (Ls × Ws × h).

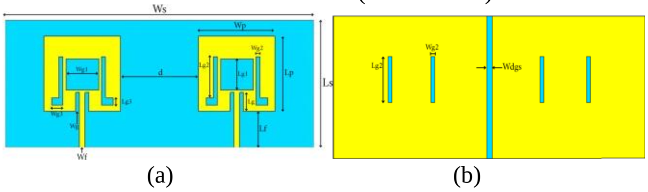

(a) (b)

Fig. 1: Geometry of the proposed dual-element MIMO antenna: (a) top view, (b) side view

2 Slot-Loaded Radiating Elements and Feeding Mechanism

Two identical slot-loaded rectangular microstrip patches serve as the primary radiating elements, as detailed in Fig. 1(a). The outer dimensions of each patch are 9.7 mm in length (Lp) and 9.9 mm in width (Wp). A key feature of the design is the integration of a rectangular slot within each patch.

The incorporation of this slot serves two primary purposes:

Precise Resonance Tuning: It enables fine adjustment of the fundamental resonant frequency to the target 27 GHz band, compensating for detuning effects caused by mutual coupling in the array environment.

Impedance Matching and Gain Enhancement: It perturbs the surface current distribution, improving the 50 Ω impedance match at the feed point and contributing to increased radiative efficiency and gain.

The patches are excited via 50 Ω microstrip transmission lines designed following standard impedance formulas for the given substrate parameters. Each feed line has a width (Wf) of 0.7 mm and a length (Lf) of 4.75 mm, providing an adequate transition from the port to the patch while maintaining impedance matching. In the simulation environment (CST Studio Suite), the feed lines are terminated with waveguide ports directly at their ends to ensure accurate excitation and S-parameter extraction.

3. Isolation Enhancement Strategy

Achieving high inter-port isolation and enhanced bandwidth in such a compact configuration necessitates a multi-faceted approach:

Adequate Spatial Separation: The two patches are positioned with an edge-to-edge separation distance (d) of 10 mm (approximately $0.093\lambda_o$ at 27 GHz, where λ_o is the free-space wavelength). This spacing provides a fundamental reduction in near-field coupling while maintaining a compact overall footprint suitable for mobile device integration.

Multiple Defected Ground Structures (DGS): The cornerstone of the isolation enhancement and bandwidth improvement is the use of five DGS elements etched into the common ground plane. This includes the original longitudinal slit (Wdgs = 0.7 mm) running parallel to the patch separation axis, centered between the two elements. Additionally, four rectangular DGS slots (each with dimensions 5.3 mm × 0.5 mm) are symmetrically distributed, two adjacent to each patch. These DGS elements function collectively to disrupt the flow of common-mode surface currents on the ground plane currents that would otherwise form the primary mutual coupling path between the two ports. By elongating and perturbing this current path more effectively, the DGS array introduces a high impedance barrier at the operating frequency, thereby significantly enhancing port-to-port isolation and improving the impedance bandwidth without severely affecting the individual radiation characteristics of each patch.

The ground plane is otherwise continuous, covering the entire bottom surface of the substrate except for the defined DGS regions. This ensures mechanical stability and maintains the integrity of the antenna's ground reference.

4 Design Methodology and Simulation Setup

To systematically evaluate the contribution of each design feature, the antenna was developed and analyzed in distinct evolutionary stages, as outlined in the next section. The final design followed a systematic parametric optimization process using CST Studio Suite 2019. Key parameters including patch dimensions (Lp, Wp), slot geometry, feed line geometry (Wf, Lf), inter-element spacing (d), and DGS width were iteratively tuned to simultaneously optimize impedance matching (S_{11}/S_{22}), inter-port isolation (S_{21}/S_{12}), and radiation performance at 27 GHz. The final dimensions, summarized in Table 1, represent the optimized configuration that balances all performance metrics.

Table 1: Dimensions of the proposed MIMO antenna

Parameter	Value(mm)	Parameter	Value (mm)
Ls	40	Lg	2.4
Ws	16.5	Wg	0.5
Lp	9.7	Lg1	3.95
Wp	9.9	Wg1	4.25
d	10	Lg2	5.3
Wf	0.7	Wg2	0.5
Lf	4.75	Lg3	1
Wdgs	0.7	Wg3	1.5
hsub	0.762	hp	0.035

5 Design Evolution: A Three-Stage Process

A clear understanding of the design's efficacy is gained by tracing its evolution through three distinct stages, illustrated in Fig. 2.

Stage A (Basic Array): This initial configuration consists of two simple, un-slotted rectangular patches with 10 mm edge-to-edge spacing on a continuous ground plane. It establishes the baseline level of mutual coupling.

Stage B (Slot-Loaded Array): This intermediate stage introduces the rectangular slots into each patch, while keeping the ground plane continuous (no DGS). This isolates the effect of patch slot-loading on individual element performance.

Stage C (Final Improved Design): This stage incorporates both key features: the slot-loaded patches from Stage B and the multiple DGS elements (one longitudinal slit and four rectangular slots) in the ground plane, along with the increased substrate thickness (0.762 mm). This represents the complete, optimized antenna with enhanced bandwidth.

This structured methodology allows us to decouple and analyze the impacts of element-level modification (slot-loading) and array-level decoupling and bandwidth enhancement (DGS and substrate tuning).

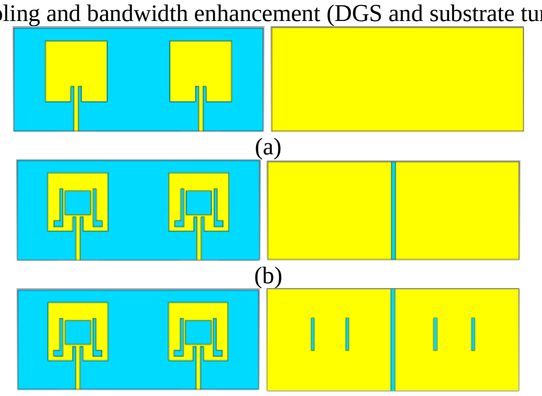

(c)

Fig. 2: The three-stage design evolution: (a) Stage A , (b) Stage B, (c) Stage C

Results and Discussion

1 S-Parameters and Bandwidth

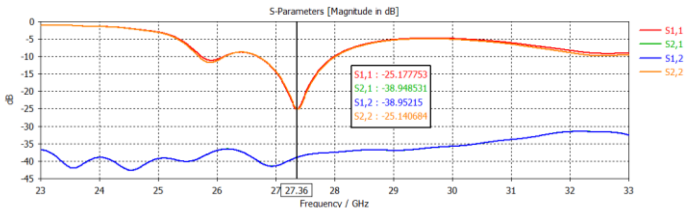

Fig. 3: Simulated S-parameters of the proposed MIMO antenna (Final Design, Stage C)

The simulated S-parameters of the final proposed antenna (Stage C) are shown in Fig.3. The reflection coefficients (|S₁₁| and |S₂₂|) reveal excellent impedance matching, with |S₁₁| reaching -25.177 dB at 27 GHz. The transmission coefficients (|S₂₁| and |S₁₂|) demonstrate high isolation performance, remaining below -30 dB across the entire 23-33 GHz band and reaching -38.948 dB at 27 GHz. This isolation is the result of the synergistic action of the slot-loaded patches and the multiple DGS elements, which effectively suppress mutual coupling by disrupting common-mode surface currents on the shared ground plane. The -10 dB impedance bandwidth is measured as 1.3126 GHz as shown in Fig 4.

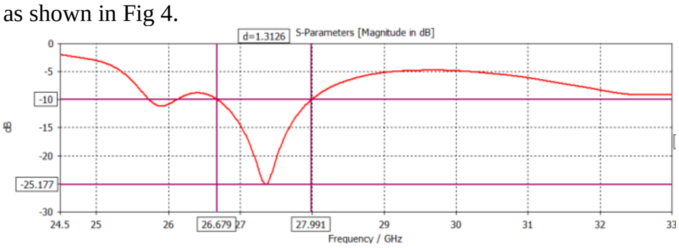

Fig. 4: Bandwidth for the final design

2 Voltage Standing Wave Ratio (VSWR)

The impedance matching is comprehensively evaluated through the Voltage Standing Wave Ratio (VSWR), as depicted in Fig. 5. The antenna exhibits outstanding impedance matching across the frequency band, with VSWR reaching remarkably low values of approximately 1.116 at 27 GHz. The operational bandwidth where VSWR < 2 is significantly enhanced compared to the initial design, comfortably encompassing the target 27 GHz 5G/6G band and beyond. This improved matching performance confirms the antenna's superior suitability for high-efficiency wideband wireless systems.

Fig. 5: Simulated Voltage Standing Wave Ratio (VSWR) for the final design

3 MIMO and Diversity Performance

The MIMO performance is critically assessed through key diversity metrics. The Envelope Correlation Coefficient (ECC), calculated from the far-field radiation patterns, is presented in Fig. 6. The ECC remains extremely low, at 3.485×10^{-7} at 27 GHz, which is significantly lower than the widely accepted threshold of 0.5 for effective MIMO operation. This ultra-low correlation confirms that the two antenna elements radiate nearly independently, enabling robust spatial diversity.

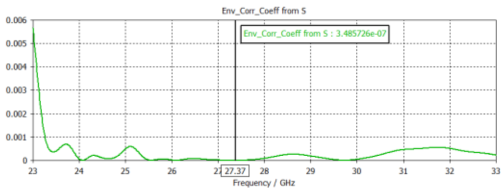

Fig. 6: Envelope Correlation Coefficient (ECC)

The Diversity Gain (DG), illustrated in Fig. 7, maintains a value of 9.99 dB at 27 GHz, virtually reaching the ideal theoretical maximum of 10 dB for a two-element diversity system. This near optimal performance further substantiates the effectiveness of the MIMO configuration in leveraging spatial diversity.

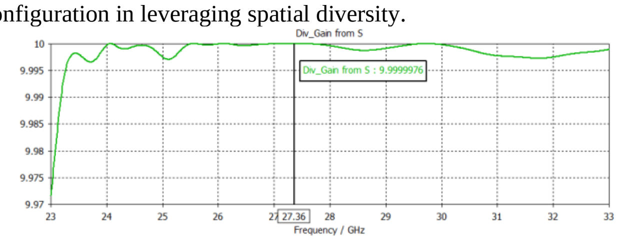

Fig. 7: Diversity Gain (DG)

The Channel Capacity Loss (CCL), shown in Fig. 8, remains below the practical limit of 0.4 bits/s/Hz around 27 GHz. This indicates that the proposed antenna introduces minimal degradation to the theoretical MIMO channel capacity, preserving the system's potential for high-data-rate transmission.

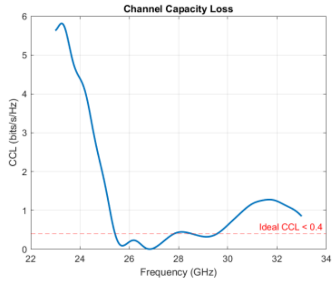

Fig. 8: Channel Capacity Loss (CCL)

The Total Active Reflection Coefficient (TARC) in Fig. 9, remains below -10 dB around 27GHz. This confirms satisfactory system-level performance when both ports are simultaneously excited, as required in practical MIMO operation scenarios.

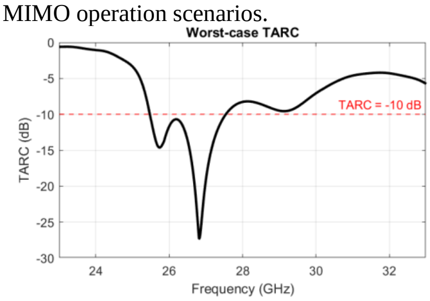

Fig. 9: Total Active Reflection Coefficient (TARC)

4 Radiation Characteristics

The normalized radiation patterns in the principal planes are shown in Figs. 10 and 11. In the H-plane (φ = 0°), the antenna exhibits a half-power beamwidth (HPBW) of 50.0° with a side lobe level (SLL) of -17.4 dB. In the E-plane (φ = 90°), the beam is narrower with an HPBW of 34.1° and an SLL of -8.6 dB. The main beam is directed at broadside, making the antenna suitable for line-of-sight communication links. The symmetric, directional radiation patterns of both elements, combined with the high inter-port isolation, render this antenna particularly well-suited for MIMO applications requiring effective spatial diversity and beamforming capabilities.

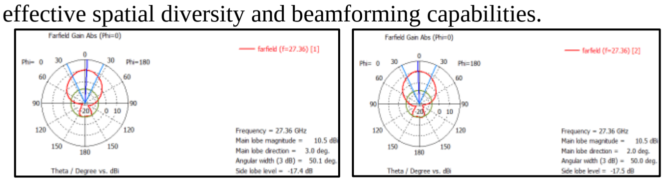

(a) (b)

Fig. 10: Normalized 2D radiation pattern in the H-plane (φ = 0°) at 27 GHz for (a) Port 1 and (b) Port 2.

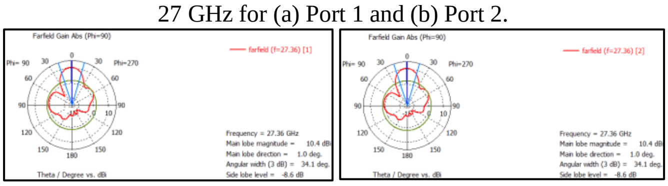

(a) (b)

Fig. 11: Normalized 2D radiation pattern in the E-plane (φ = 90°) at 27 GHz for (a) Port 1 and (b) Port 2.

The radiation characteristics of both antenna elements at 27 GHz are summarized in Table 2. Each element exhibits nearly identical performance, confirming the design symmetry essential for balanced MIMO operation.

Table 2: Radiation Characteristics at 27 GHz

Parameter	Value
Peak Gain	10.45 dBi
Directivity	11.49 dBi
Radiation Efficiency	78.8%

Parameter	Value
Total Efficiency	78.5%
H-plane HPBW (φ=0°)	50.0°
E-plane HPBW (φ=90°)	34.1°
H-plane Side Lobe Level	-17.4 dB
E-plane Side Lobe Level	-8.6 dB

5 Comparative Analysis: Isolating the Impact of Slots and DGS

The effectiveness of the combined design strategy is unequivocally demonstrated by comparing the performance of the three evolutionary stages. Table 3 summarizes the key metrics at the primary design frequency (27 GHz).

At 27 GHz, the improved final design (Stage C) shows excellent impedance matching (S_{11} = -25.177 dB) and maintains high isolation (S_{21} = -35.948 dB). The gain is slightly reduced compared to the previous Stage C design due to the increased substrate thickness and modified DGS configuration, which were traded for a significant enhancement in bandwidth.

Slot-loading remains essential for achieving the correct operating frequency and a viable impedance match. The multiple DGS elements, combined with increased substrate thickness, are then introduced to ensure high isolation and, crucially, a significantly enhanced impedance bandwidth in the MIMO array. The final improved design (Stage C) successfully integrates both: it operates at the 27 GHz target, maintains excellent matching (VSWR = 1.11), delivers good gain and efficiency, provides robust isolation (>38 dB), and achieves an improved bandwidth of 1.3124 GHz with exceptional diversity performance (ECC = 3.485×10^{-7}, DG = 9.99 dB). This demonstrates that element-level optimization (slots) and array-level decoupling/bandwidth enhancement (multiple DGS and substrate tuning) are complementary strategies that address distinct challenges in compact wideband mmWave MIMO design.

The design of MIMO antennas with high isolation, compact dimensions, and wide bandwidth remains a critical challenge in 5G/6G systems. Several techniques have been explored to suppress mutual coupling, among which defected ground structures (DGS) and decoupling elements have shown promising results. Previous studies, such as those reported in [22−27], have employed various isolation enhancement methods for diversity MIMO configurations, with key performance metrics summarized in Table 4. The proposed antenna in this work further advances these efforts by achieving high isolation alongside a significantly improved impedance bandwidth, while maintaining a compact footprint. Notably, the design delivers excellent diversity performance despite its miniaturized structure.

The antenna presented here balances performance, size, bandwidth, and simplicity, making it suitable for compact 5G/6G devices.

Table 3: Performance Comparison of Design Stages at 27 GHz

Parameter	Stage A	Stage B	Stage C
S_{11} (dB)	-24.064	-24.039	-25.177
S_{21} (dB)	-38.31	-44.892	-38.948
VSWR	2.4304	1.1488	1.116
Peak Gain (dBi)	9.113	10.96	10.45
Directivity	10.57	11.89	11.49
ECC	1.5752×10^{-4}	3.3614×10^{-7}	3.485×10^{-7}

Table 4: Comparative study of different 5G MIMO antennas

Reference	Dimensions (mm^3)	Mutual coupling (dB)	Resonant frequency (GHz)	Gain (dB)	ECC	DG
[22]	(20×40×1.6)	-29.34	28 GHz	7	0.005	9.95
[23]	(28×16×6.3)	-33	40GHz	10	0.1	9.98
[24]	(26×14.5×0.508)	-39 at 28 GHz -39 at 38 GHz	28 and 38 GHz	5.2 at 28 GHz and 5.5 at 38 GHz	0.001	9.98
[25]	NA	-35	4.95 GHz	10.6	NA	NA
[26]	NA	-35	10 GHz	13.5	NA	NA
[27]	(28×14×1.6)	-40 at 28 GHz -42 at 38 GHz	28 and 38 GHz	6.2 at 28 GHz and 7 at 38 GHz	0.0015	9.99
This work	(40×16.5×0.832)	-38 at 27GHz	27 GHz	10.45	3.485×10^{-7}	9.99

Conclusion and Future Work

In this work, we have designed and analyzed a compact, dual element MIMO antenna for the 27 GHz band using a dual modification strategy enhanced with multiple DGS and increased substrate thickness. The evolutionary analysis proved critical: slot loading the radiating patches was essential to correct a severe broadband impedance mismatch and to tune the fundamental resonance to the target frequency. Subsequently, an array of five Defected Ground Structures (DGS) combined with a substrate thickness of 0.762 mm were integrated to provide high inter-port isolation (>38 dB at 27 GHz) and, most importantly, to achieve a significantly enhanced impedance bandwidth of 1.3124 GHz while maintaining near-ideal MIMO diversity performance (ECC = 3.485×10^{-7}, DG = 9.99 dB).

The key insight is that these simple, planar features address different layers of the design problem. The slots ensure each antenna element is efficient, well-matched, and operates at the correct frequency. The multiple DGS elements and increased substrate thickness ensure these well-tuned elements can function independently in a closely spaced array while offering wider operational bandwidth. This synergy results in a high-performance antenna with a gain of 10.45 dBi, total efficiency of approximately 78.5%, and excellent matching fabricated in a single-layer PCB process, offering a compelling balance of performance, bandwidth, and manufacturability for 5G/6G user equipment.

Future work will focus on: fabricating a prototype to validate the simulated performance, especially the enhanced broadband match; and extending this slot-and-multiple-DGS methodology to larger MIMO arrays (e.g., 4-element); and investigating the impact of DGS geometry variations on the trade-off between bandwidth, gain, and isolation; and integrating the antenna with an RF front-end for system-level evaluation in a communication link.

Abbreviations and Acronyms

MIMO – Multiple-Input Multiple-Output
DGS – Defected Ground Structure
mmWave – millimeter-wave
ECC – Envelope Correlation Coefficient
VSWR – Voltage Standing Wave Ratio
HPBW – Half-Power Beamwidth
5G – Fifth Generation
6G – Sixth Generation
FCC – Federal Communications Commission
3GPP – 3rd Generation Partnership Project
NR – New Radio
UE – User Equipment
EBG – Electromagnetic Band-Gap
CMA – Characteristic Mode Analysis
PCB – Printed Circuit Board
DG – Diversity Gain
CCL – Channel Capacity Loss
TARC – Total Active Reflection Coefficient
SLL – Side Lobe Level
SIW – Substrate Integrated Waveguide

References

[1] Andrews, J. G., et al., (2014), What will 5G be?, IEEE J. Sel. Areas Commun., 32, 1065–1082. DOI: 10.1109/JSAC.2014.2328098 .

[2] Jiang, W., Han, B., Habibi, M. A., Schotten, H. D., (2021), The road towards 6G: A comprehensive survey, IEEE Open J. Commun. Soc., 2, 334–366. DOI: 10.1109/OJCOMS.2021.3057679 .

[3] Rappaport, T. S., Xing, Y., Kanhere, O., Ju, S., Madanayake, A., Mandal, S., (2019), Wireless communications and applications above 100 GHz: Opportunities and challenges for 6G and beyond, IEEE Access, 7, 78729–78757. DOI: 10.1109/ACCESS.2019.2921522 .

[4] Gesbert, D., Shafi, M., Shiu, D., Smith, P. J., Naguib, A., (2003), From theory to practice: An overview of MIMO space-time coded wireless systems, IEEE J. Sel. Areas Commun., 21, 281–302. DOI: 10.1109/JSAC.2003.809458

[5] Rangan, S., Rappaport, T. S., Erkip, E., (2014), Millimeter-wave cellular wireless networks: Potentials and challenges, Proc. IEEE, 102, 366–385. DOI:10.1109/JPROC.2014.2299397.

[6] Federal Communications Commission (FCC), Spectrum Frontiers Report and Order (FCC 16-89); Federal Communications Commission, Washington, DC, USA. 2016

[7] Sharawi, M. S., (2014), Printed MIMO antenna systems: Performance metrics, implementations and challenges, Forum Electromagn. Res. Methods Appl. Technol., 1, 1–11. DOI: 10.13140/2.1.1247.2966 .

[8] Zhang, S., Pedersen, G. F., Pedersen, M. O. J. A. E. G. F., (2016), Mutual coupling reduction for UWB MIMO antennas with a wideband neutralization line, IEEE Antennas Wireless Propag. Lett., 15, 166–169. DOI:10.1109/LAWP.2015.2435992.

[9] Yang, F., Rahmat-Samii, Y., (2003), Microstrip antennas integrated with electromagnetic band-gap (EBG) structures: A low mutual coupling design for array applications, IEEE Trans. Antennas Propag., 51, 2936–2946. DOI: 10.1109/TAP.2003.817983.

[10] Jafargholi, A., Jafargholi, A., Choi, J. H., (2019), Mutual coupling reduction in an array of patch antennas using CLL metamaterial superstrate for MIMO applications, IEEE Trans. Antennas Propag., 67, 179–189. DOI: 10.1109/TAP.2018.2874747.

[11] Chiu, C.-Y., Cheng, C.-H., Murch, R. D., Rowell, C. R., (2007), Reduction of mutual coupling between closely-packed antenna elements, IEEE Trans. Antennas Propag., 55, 1732–1738. DOI: 10.1109/TAP.2007.898618.

[12] Wei, K., Li, J.-Y., Wang, L., Xing, Z.-J., Xu, R., (2016), Mutual coupling reduction by novel fractal defected ground structure bandgap filter, IEEE Trans. Antennas Propag., 64, 4328–4335. DOI: 10.1109/TAP.2016.2591058.

[13] Gao, D., Cao, Z.-X., Fu, S.-D., Quan, X., Chen, P., (2020), A novel slot-array defected ground structure for decoupling microstrip antenna array, IEEE Trans. Antennas Propag., 68, 7027–7038. DOI: 10.1109/TAP.2020.2992881.

[14] Li, M., Jiang, L., Yeung, K. L., (2020), A general and systematic method to design neutralization lines for isolation enhancement in MIMO antenna arrays, IEEE Trans. Veh. Technol., 69, 6242–6253. DOI: 10.1109/TVT.2020.2984044.

[15] Tran, H. H., Nguyen-Trong, N., (2021), Performance enhancement of MIMO patch antenna using parasitic elements, IEEE Access, 9, 30011–30016. DOI: 10.1109/ACCESS.2021.3058340.

[16] Li, M., Zhang, Y., Wu, D., Yeung, K. L., Jiang, L., Murch, R., (2022), Decoupling and matching network for dual-band MIMO antennas, IEEE Trans. Antennas Propag., 70, 1764–1775. DOI: 10.1109/TAP.2021.3118791.

[17] Sun, L., Li, Y., Zhang, Z., (2021), Decoupling between extremely closely spaced patch antennas by mode cancellation method, IEEE Trans. Antennas Propag., 69, 3074–3083. DOI: 10.1109/TAP.2020.3030922.

[18] Lai, Q. X., Pan, Y. M., Zheng, S. Y., Yang, W. J., (2021), Mutual coupling reduction in MIMO microstrip patch array using TM_{10} and TM_{02} modes, IEEE Trans. Antennas Propag., 69, 7562–7571. DOI:10.1109/TAP.2021.3090520.

[19] Lai, Q. X., Pan, Y. M., Zheng, S. Y., (2023), A self-decoupling method for MIMO antenna array using characteristic mode of ground plane, IEEE Trans. Antennas Propag., 71, 2126–2135. DOI: 10.1109/TAP.2023.3240561.

[20] Elahi, M., Koziel, S., Leifsson, L., (2025), Self-isolation in MIMO microstrip patch arrays using annular via-based mode conversion, IEEE Access, 13, 107467–107480. DOI: 10.1109/ACCESS.2025.3549619.

[21] Lee, K. F., Luk, K. M., Tong, K. F., Shum, S. M., Huynh, T., Lee, R. Q., (1997), Experimental and simulation studies of the coaxially fed U-slot rectangular patch antenna, IEE Proc.-Microw. Antennas Propag., 144, 354–358. DOI: 10.1049/ip-map:19971334.

[22] Park, J.-D., Rahman, M., Chen, H. N., (2019), Isolation enhancement of wide-band MIMO array antennas utilizing resistive loading, IEEE Access, 7, 81020–81026. DOI: 10.1109/ACCESS.2019.2923330.

[23] Khajeh-Khalili, F., Honarvar, M. A., Naser-Moghadasi, M., Dolatshahi, M., (2020), Gain enhancement and mutual coupling reduction of multiple-input multiple-output antenna for millimeter-wave applications using two types of novel metamaterial structures, International Journal of RF and Microwave Computer-Aided Engineering, 30, e22006. DOI: 10.1002/mmce.22006

[24] Esmail, B. A., Koziel, S., (2023), High isolation metamaterial-based dual-band MIMO antenna for 5G millimeter-wave applications, AEU – International Journal of Electronics and Communications, 158, 154470. DOI:10.1016/j.aeue.2022.154470.

[25] Diman, A. A., Karami, F., Rezaei, P., Amn-E-Elahi, A., Mousavirazi, Z., Denidni, T. A., Kishk, A. A., (2021), Efficient SIW-feed network suppressing mutual coupling of slot antenna array, IEEE Transactions on Antennas and Propagation, 69, 6058–6063. DOI:10.1109/TAP.2021.3069557.

[26] Nimehvari Varcheh, H., Rezaei, P., (2022), Integration of the modified butler matrix and decoupling network for beam-steering antenna array, International Journal of RF and Microwave Computer-Aided Engineering, 32, e23015. DOI: 10.1002/mmce.23015.

[27] Thakur, E., Gupta, A., Abdulhameed, M. K., Khaleel, A. D., Al-Gburi, A. J. A., (2024), Microstrip Antenna with Two Elements and Defected Ground Structure for 5G Mobile Applications at 28/38 GHz, Progress In Electromagnetics Research C, 146, 177–185. DOI: 10.2528/PIERC24062403.